RESEARCH ARTICLE
PLANETARY SCIENCES

Earth and Planetary Physics
9: 541–549, 2025
doi: 10.26464/epp2025013

Influence of different data selection criteria on internal geomagnetic field modeling

HongBo Yao*, **JuYuan Xu, Yi Jiang, Qing Yan, Liang Yin, and PengFei Liu**

Macau Institute of Space Technology and Application, Macau University of Science and Technology, Macao 999078, China

Key Points:

- The influence of different data selection criteria on internal geomagnetic field modeling was quantitatively investigated.
- The Macau Science Satellite-1 (MSS-1) and Swarm satellite magnetic data were used for our investigations.
- These investigations would provide a crucial reference for constructing and applying geomagnetic field models.

Citation: Yao, H. B., Xu, J. Y., Jiang, Y., Yan, Q., Yin, L., and Liu, P. F. (2025). Influence of different data selection criteria on internal geomagnetic field modeling. *Earth Planet. Phys.*, *9*(3), 541–549. http://doi.org/10.26464/epp2025013

Abstract: Earth's internal core and crustal magnetic fields, as measured by geomagnetic satellites like MSS-1 (Macau Science Satellite-1) and Swarm, are vital for understanding core dynamics and tectonic evolution. To model these internal magnetic fields accurately, data selection based on specific criteria is often employed to minimize the influence of rapidly changing current systems in the ionosphere and magnetosphere. However, the quantitative impact of various data selection criteria on internal geomagnetic field modeling is not well understood. This study aims to address this issue and provide a reference for constructing and applying geomagnetic field models. First, we collect the latest MSS-1 and Swarm satellite magnetic data and summarize widely used data selection criteria in geomagnetic field modeling. Second, we briefly describe the method to co-estimate the core, crustal, and large-scale magnetospheric fields using satellite magnetic data. Finally, we conduct a series of field modeling experiments with different data selection criteria to quantitatively estimate their influence. Our numerical experiments confirm that without selecting data from dark regions and geomagnetically quiet times, the resulting internal field differences at the Earth's surface can range from tens to hundreds of nanotesla (nT). Additionally, we find that the uncertainties introduced into field models by different data selection criteria are significantly larger than the measurement accuracy of modern geomagnetic satellites. These uncertainties should be considered when utilizing constructed magnetic field models for scientific research and applications.

Keywords: Macau Science Satellite-1; Swarm; geomagnetic field modeling; data selection; core field; crustal field

1. Introduction

The Macau Science Satellite-1 (MSS-1) is the world's first geomagnetic satellite mission with a low inclination of 41°. It was successfully launched on May 21, 2023, into near-circular orbits at an altitude of 450 km (Zhang K, 2023). MSS-1 is equipped with a highly stable optical bench, a high-precision fluxgate magnetometer, and a high-precision scalar magnetometer. It can measure Earth's magnetic field with unprecedented accuracy and provides excellent local time sampling. Combined with magnetic data from the Swarm satellite (Olsen et al., 2013), MSS-1 will significantly advance the relevant scientific research and applications.

Magnetic field measurements include both external and internal sources relative to the Earth's surface. The internal field primarily consists of the core and crustal fields, while the external field originates from current systems in the ionosphere and magnetosphere. The core field dominates on large spatial scales and exhibits secular variations (SV), while the static crustal field dominates on smaller spatial scales. Analyzing these internal fields provides crucial insights into core dynamics (Olsen and Mandea, 2008; Li JF et al., 2024) and tectonic evolution (Purucker et al., 2002; Wang J et al., 2024). Additionally, internal fields offer position and direction information for geomagnetic heading and navigation systems (Maus et al., 2012; Chulliat et al., 2020). Constructing a geomagnetic field model that accurately represents the temporal and spatial variations of Earth's internal magnetic field is essential for these applications. However, internal geomagnetic field models are influenced by rapidly varying current systems in the ionosphere and magnetosphere (Finlay et al., 2017). To reduce these effects, a common practice is to select magnetic data from dark regions during geomagnetically quiet times based on specific criteria (Olsen et al., 2006; Maus et al., 2010; Lesur et al., 2015; Finlay et al., 2020; Sabaka et al., 2020; Yang YY et al., 2021). Nevertheless, the quantitative impact of different data selection criteria on internal geomagnetic field modeling is not well studied and requires further investigation.

This study combines the latest MSS-1 and Swarm satellite magnetic data to examine how different data selection criteria

Correspondence to: H. B. Yao, hongbo.yao@outlook.com
Received 29 OCT 2024; Accepted 30 DEC 2024.
First Published online 14 JAN 2025.

affect internal geomagnetic field modeling. The aims are: (i) to quantify the impact of sunlit and geomagnetically disturbed data on the internal geomagnetic field models; (ii) to quantify model uncertainties caused by different data selection criteria; and (iii) to provide a reference for data selection in internal geomagnetic field modeling. The manuscript is structured as follows: Section 2 describes the data selection criteria and the method of internal geomagnetic field modeling. Section 3 presents the field modeling setups and results. Section 4 summarizes the findings and conclusions.

2. Data and Method

2.1 Data Selection

The MSS-1 and Swarm satellite magnetic data are used for our investigations. For the MSS-1 satellite, we use vector data from November 1, 2023, to August 31, 2024. For the Swarm satellite, we use vector data from January 1, 2014, to August 31, 2024. At high latitudes, Swarm scalar data are also used. The sampling interval for these data is 1 minute. To select dark-region data from geomagnetically quiet times, the following criteria are commonly applied in the widely used CHAOS geomagnetic model series (Olsen et al., 2006, 2014; Finlay et al., 2020):

(1) Only data from dark regions (sun at least 10° below the horizon) are used. This criterion excludes data influenced by low and middle ionospheric current systems due to solar heating, as ionospheric current fields are not parametrized in the field modeling (see Section 2.2).

(2) Vector data are used for quasi-dipole latitudes equatorward of ±55°, while scalar data are used for quasi-dipole latitudes poleward of ±55°. This criterion is based on the fact that scalar data are less affected by polar current systems (Friis-Christensen et al., 2017).

(3) The 3-hour planetary *K* index (Matzka et al., 2021) $Kp \le 2°$. This criterion excludes data during periods of enhanced geomagnetic fluctuations.

(4) The magnetospheric ring current index *RC* (Olsen et al., 2014) changes by at most 2 nT/h, i.e., $|dRC/dt| \le 2$ nT/h. This criterion excludes data during periods of enhanced ring current activity.

(5) The merging electric field E_m (Newell et al., 2007) averaged over the previous 2 h is no more than 0.8 mV/m, i.e., $E_m \le$ 0.8 mV/m. This criterion excludes data during periods of enhanced activity in polar regions.

(6) Interplanetary magnetic field (IMF) B_z averaged over the previous 2 h is positive. This criterion excludes data disturbed due to substorm auroral electrojet, which is prominent when IMF $B_z < 0$ (Finlay et al., 2015).

As an illustration, Figure 1 shows the monthly number of selected MSS-1 and Swarm magnetic data points based on the above data selection criteria. In this work, the above criteria are used as a reference. We will change the threshold values of these indices to investigate their influence on internal geomagnetic field modeling.

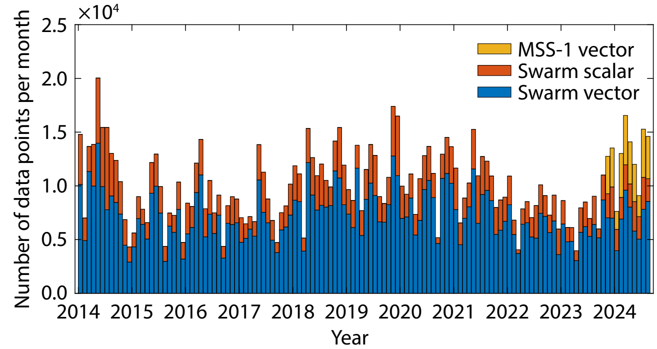

Figure 1. Stacked histogram of the monthly number of MSS-1 and Swarm magnetic data points selected by the data selection criteria described in Section 2.1.

2.2 Internal Geomagnetic Field Modeling

We employ a newly developed framework (Yao HB et al., 2025) for geomagnetic field modeling. This framework co-estimates the core, crustal, and large-scale magnetospheric fields. In source-free regions, the magnetic field $\boldsymbol{B} = -\nabla V$ is derived from a magnetic scalar potential V, which consists of an internal part V^{int} for core and crustal fields, and an external part V^{ext} for magnetospheric and their Earth mantle-induced fields. The internal part V^{int} is described by spherical harmonic (SH) expansion in Earth-centered, Earth-fixed coordinate system (Olsen et al., 2006):

$$V^{\text{int}} = a\sum_{n=1}^{N_{\text{int}}}\sum_{m=0}^{n}(g_n^m\cos m\phi + h_n^m\sin m\phi)\left(\frac{a}{r}\right)^{n+1}P_n^m(\cos\theta), \tag{1}$$

where a = 6371.2 km is the Earth's mean radius, r, θ, and ϕ represent the radius, colatitude, and longitude, respectively, $P_n^m(\cos\theta)$ is the Schmidt quasi-normalized associated Legendre function of degree n and order m (Winch et al., 2005), N_{int} = 50 is the maximum degree used to describe the internal field, and g_n^m and h_n^m are the SH model coefficients. Coefficients up to degree n = 20 represent the time-dependent core field. The time dependence of the secular variation of the core field is represented by order-6 B-splines (De Boor, 2001) with 6-month knot intervals and fivefold knots at the endpoints t = 2014.0 and t = 2025.0. Coefficients for degrees n = 21 – 50 are time-independent and represent the static crustal field. Details on the external part V^{ext} due to the magnetospheric ring current, magnetotail current, and magnetopause current can be found in Yao HB et al. (2025). The unknown model parameters are the SH coefficients for the core, crust, and magnetospheric fields. The total number of model parameters is 15,083.

Model parameters $\boldsymbol{m}$ are estimated by minimizing the following objective function (Olsen et al., 2014):

$$\phi(\boldsymbol{m}) = \boldsymbol{e}^{\text{T}}\boldsymbol{C}_d^{-1}\boldsymbol{e} + \lambda_3\boldsymbol{m}^{\text{T}}\boldsymbol{\Lambda}_3\boldsymbol{m} + \lambda_2\boldsymbol{m}^{\text{T}}\boldsymbol{\Lambda}_2\boldsymbol{m}, \tag{2}$$

where $\boldsymbol{e} = \boldsymbol{d}_{\text{obs}} - \boldsymbol{d}_{\text{mod}}$ is the data residual vector with $\boldsymbol{d}_{\text{obs}}$ and $\boldsymbol{d}_{\text{mod}}$ denoting the observed and model predicted magnetic data vectors in the north-east-centre coordinate system; $\boldsymbol{C}_d^{-1}$ is the inverse of the data error covariance matrix considering the anisotropic errors due to attitude uncertainty (Olsen, 2002); $\boldsymbol{\Lambda}_3$ and $\boldsymbol{\Lambda}_2$ are the block diagonal damping matrices that constrain the third and second-time derivatives of the core field, respectively (Olsen et al., 2014); λ_3 and λ_2 control the strength of damping. Following Finlay et al. (2015), we take $\lambda_3 = 0.33\,(\text{nT yr}^{-3})^{-2}$ and $\lambda_2 = 100\,(\text{nT yr}^{-2})^{-2}$ and treat all zonal terms g_n^0 separately with λ_3 increased to $100\,(\text{nT yr}^{-3})^{-2}$. The influence of regularization on the geomagnetic core field modeling can be seen in the work of Xu JY et al. (2024). To minimize the objective function, we implemented an iteratively reweighted least squares method with Huber weights (Constable, 1988) and Gauss-Newton iteration (Farquharson and Oldenburg, 1998; Olsen, 2002). For more details, we refer to Yao HB et al. (2025).

3. Numerical Experiments

3.1 Setup

To illustrate the influence of data selection on internal geomagnetic field modeling, we generated nine geomagnetic field models based on data selected according to different criteria. Hereafter, an internal core and crust magnetic field model up to SH degree n = 50 as predicted by the CHAOS-7 model (Finlay et al., 2020) at epoch t = 2020.0 was used as the initial model of inversion iteration. The inversion converges when the root-mean-square (RMS) misfit difference between adjacent iterations is less than 10^{-2}. All numerical experiments were conducted using 90 MPI cores at the High-Performance Computing Center of MSS-1.

Table 1 lists the data selection parameters. Model 0 is the reference model. The purposes of the other numerical experiments are summarized as follows:

(1) Model 1 incorporates data from both dark and sunlit regions to quantify the influence of sunlit data on internal geomagnetic field modeling.

(2) Model 2 includes data without selecting geomagnetically quiet times to evaluate the effect of geomagnetically disturbed data.

(3) Models 3 and 4 utilize data during periods of weak and strong geomagnetic fluctuations, respectively, based on the Kp index.

(4) Models 5 and 6 employ data during weak and strong ring current activities, respectively, as indicated by the RC index.

(5) Models 7 and 8 explore the influence of data selection criteria based on the merging electric field E_m and the interplanetary magnetic field B_z. These indices help exclude data from periods of enhanced activity in polar regions.

3.2 Influence of Sunlit and Geomagnetically Disturbed Data

Selecting dark-region and geomagnetically quiet-time data is a standard criterion in geomagnetic field modeling, but its influence on internal geomagnetic field modeling is not quantified. Here, we first use Model 1 to investigate the influence of sunlit data (no dark-region selection). Table 2 lists the Huber-weighted residual mean and RMS misfit (Olsen et al., 2009) for the experiments. Compared to the reference Model 0 derived from only dark-region data, the RMS misfits of Model 1 increase distinctly for all field components. The higher RMS of Model 1 may indicate unmodelled ionospheric fields since this model includes sunlit data, which are affected by the ionospheric equatorial electrojet (EEJ) and Sq current systems.

Figures 2 and 3 present the spherical harmonic spectra and maps of the core and crustal fields at the Earth's surface and epoch t = 2024.5 for the reference Model 0 and the differences between various models. Compared to Model 0, obvious spectra differences are observed for Model 1, especially for the high-degree core SV field and crustal field. In the middle row of Figure 3, the field differences between Model 1 and Model 0 display remarkable small-scale structure alone magnetic equator. A similar result was obtained by Finlay et al. (2017). This is a characteristic of the EEJ, demonstrating the leakage of the unmodeled EEJ field. As shown in the middle row of Figure 3, the field differences due to the use of sunlit data are larger than 10 nT.

Table 1. Model setups using different data selection criteria. The transverse line means no application of this criterion. Differences compared to the reference Model 0 are highlighted in bold font.

Model	Kp	$\lvert dRC/dt \rvert$	E_m	IMF B_z	Region	Vector data	Scalar data
0	≤ 2°	≤ 2 nT/h	≤ 0.8 mV/m	> 0	dark	963,762	324,790
1	≤ 2°	≤ 2 nT/h	≤ 0.8 mV/m	> 0	**dark+sunlit**	2,039,268	811,109
2	–	–	–	–	dark	1,457,028	1,501,922
3	**≤ 1°**	≤ 2 nT/h	≤ 0.8 mV/m	> 0	dark	701,364	238,880
4	**≤ 3°**	≤ 2 nT/h	≤ 0.8 mV/m	> 0	dark	1,027,259	344,337
5	≤ 2°	**≤ 1 nT/h**	≤ 0.8 mV/m	> 0	dark	563,675	189,947
6	≤ 2°	**≤ 3 nT/h**	≤ 0.8 mV/m	> 0	dark	1,191,697	400,826
7	≤ 2°	≤ 2 nT/h	–	> 0	dark	1,118,549	377,652
8	≤ 2°	≤ 2 nT/h	≤ 0.8 mV/m	–	dark	1,170,766	397,340

Table 2. Huber weighted residual mean, and RMS misfit for magnetic field Models 0, 1 and 2.

Field	Model 0		Model 1		Model 2	
	Mean	RMS	Mean	RMS	Mean	RMS
F	−0.01	3.39	0.04	5.02	−0.10	8.90
B_r	0.06	1.83	0.02	4.01	0.05	3.04
B_θ	0.01	2.62	−0.12	4.12	−0.15	5.53
B_ϕ	−0.04	2.26	−0.05	5.11	−0.08	4.68

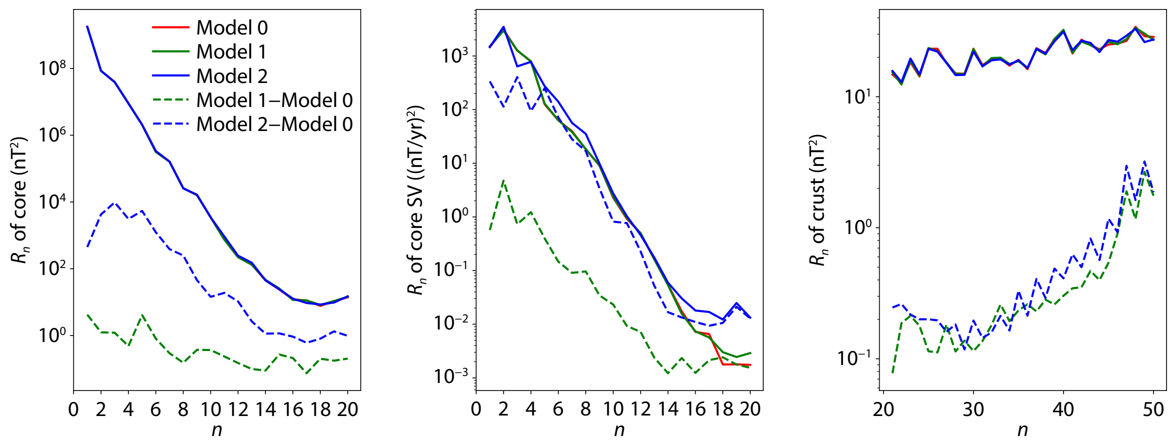

Figure 2. Spherical harmonic spectra (R_n) of the core field (left), core SV field (middle), and crustal field (right) at the Earth's surface and epoch t = 2024.5 for magnetic field Models 0, 1, and 2, respectively.

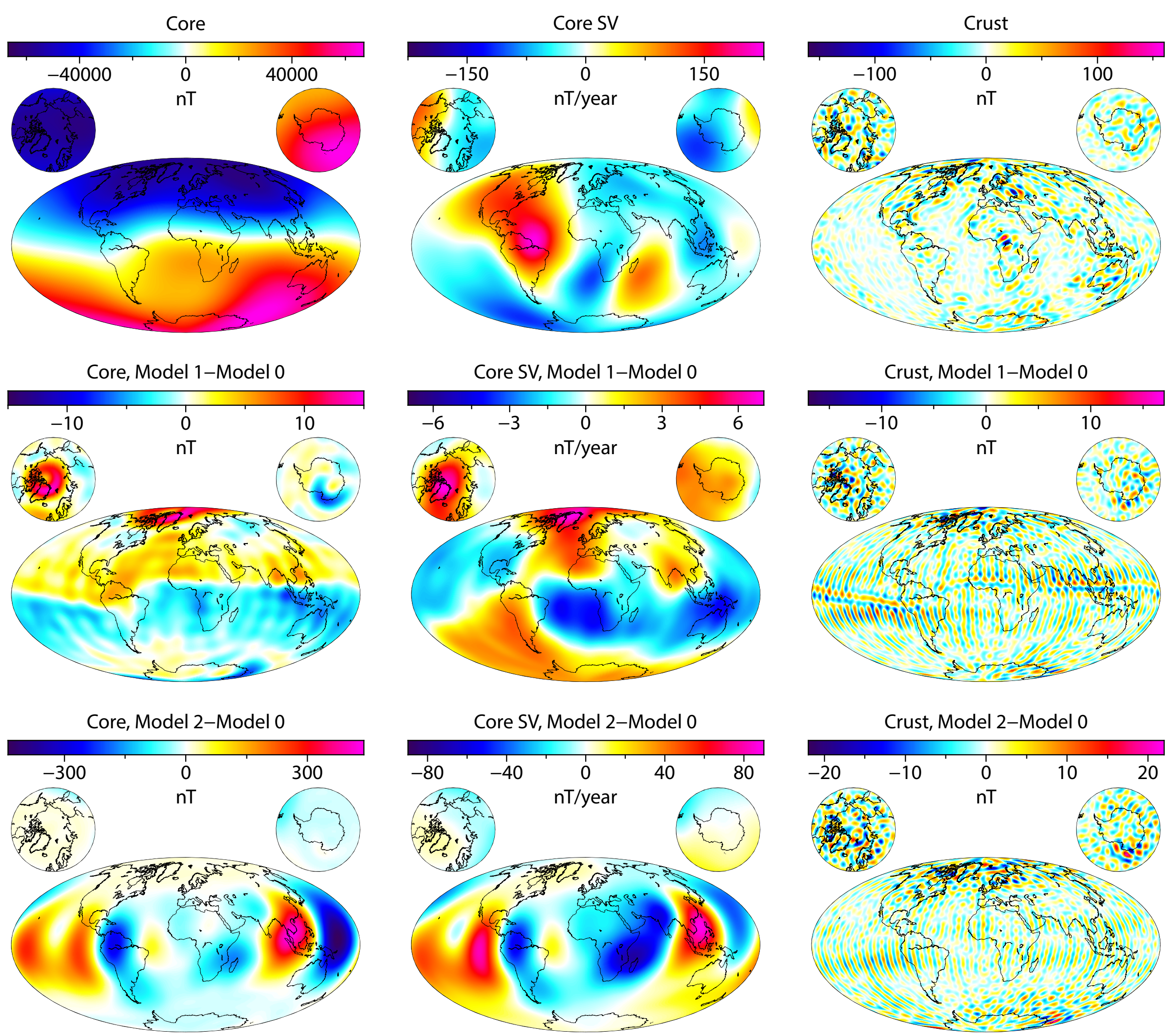

Figure 3. Maps of the radial core field (left, n = 1−20), core SV field (middle, n = 1−20), and crustal field (right, n = 21−50) at the Earth's surface and epoch t = 2024.5. Top row: maps for Model 0; middle row: differences between Model 1 and Model 0; bottom row: differences between Model 2 and Model 0.

We further use Model 2 to quantify the influence of geomagnetically disturbed data (no quiet-time selection). Results for this model are also presented in Table 2, Figures 2 and 3. Compared to Model 0, the RMS misfits of Model 2 increase significantly. As seen in Figure 2, the spectra differences between Model 2 and Model 0 are significantly larger. The magnitude of spectra differences are even larger than those of spectra themselves for the core SV field. In the bottom row of Figure 3, we observe very large field differences between Model 2 and Model 0, which can reach several hundreds of nT. The spatial structure of the core field and SV field differences is dominated by east-west aligned features at middle latitudes.

During geomagnetically disturbed times, there is enhanced interaction between the solar wind and Earth's magnetosphere, resulting in rapid disturbances of the Earth's magnetosphere. These disturbance magnetic fields can reach an order of several hundreds of nT (Yan Q and Yao HB, 2024). Since the sunlit data are excluded, the mid-latitude ionospheric field contribution is minimized. The large differences are most probably caused by the leakage of magnetospheric disturbance fields during strong geomagnetic activity. These results demonstrate quantitatively the importance of selecting geomagnetically quiet-time data for accurate geomagnetic field modeling when using spherical harmonic methods. They also suggest that the spherical harmonic model can hardly explain the observed magnetic fields during strong geomagnetic activity. Therefore, we need a more sophisticated approach to better parameterize the external fields.

3.3 Influence of Data Selection According to *Kp* Index

Next, we investigate the influence of data selection according to *Kp* index. We tested three data sets selected by $Kp \le 2°$ (Model 0, reference), $Kp \le 1°$ (Model 3, stricter criterion), and $Kp \le 3°$ (Model 4, looser criterion). Residual statistics for these tests are recorded in Table 3. It is observed that a stricter data selection criterion leads to lower RMS misfits while a looser data selection criterion leads to higher RMS misfits. This result is expected since a looser data selection criterion includes much more geomagnetically disturbed data, which can not be accurately modeled.

Figures 4 and 5 present the spherical harmonic spectra of Models 0, 3, and 4 and field differences between various models. For the core field and the crustal field, the spectra differences occurred mainly at high SH degrees (correspond to small spatial scales), which is consistent with the small-scale field differences shown in the left and right panels of Figure 5. It is also observed that the field differences between Model 3 (stricter criterion) and Model 0 are distinctly larger than those between Model 4 (looser criterion) and Model 0. This result may suggest that stricter data selection is not always better since we may lose small-scale information by excluding too much data.

In the following sections, we will not study the trade-off between data selection and model spatial resolution, but focus on the estimation of uncertainties introduced into the model by different data selection criteria. The estimated uncertainties provide a reference for analyzing and applying the magnetic field model. When changing the *Kp* index by 50% in data selection, the model uncertainties are in the ranges of ±3 nT, ±3 nT/year, and ±6 nT for the core, core SV, and crustal fields, respectively. These uncertainties should be considered when using the constructed magnetic field models for relevant scientific research and applications.

Table 3. Similar to Table 2, but for magnetic field Models 0, 3 and 4.

Field	Model 0		Model 3		Model 4	
	Mean	RMS	Mean	RMS	Mean	RMS
F	−0.01	3.39	0.02	2.92	−0.02	3.61
B_r	0.06	1.83	0.06	1.75	0.07	1.88
B_θ	0.01	2.62	0.02	2.38	0.00	2.75
B_ϕ	−0.04	2.26	−0.03	2.08	−0.04	2.34

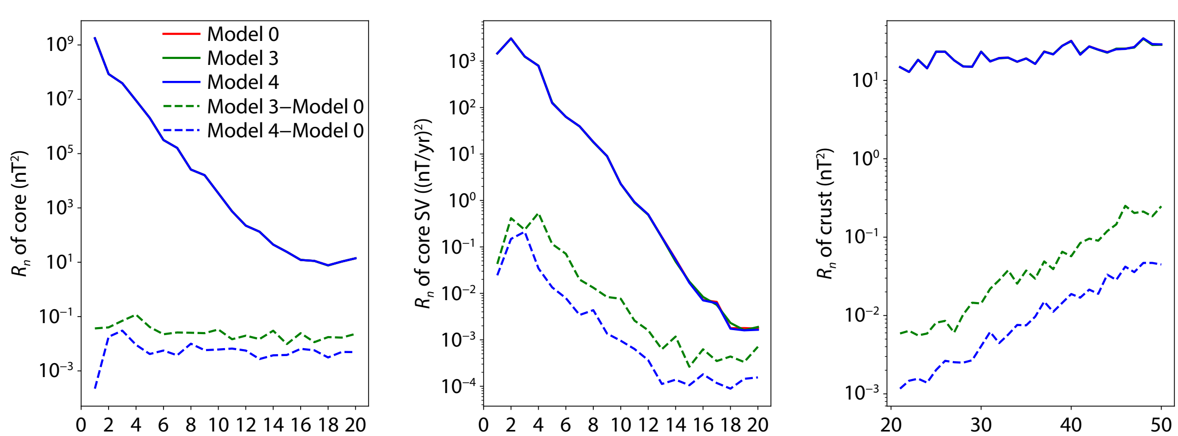

Figure 4. Similar to Figure 2, but for magnetic field Models 0, 3, and 4.

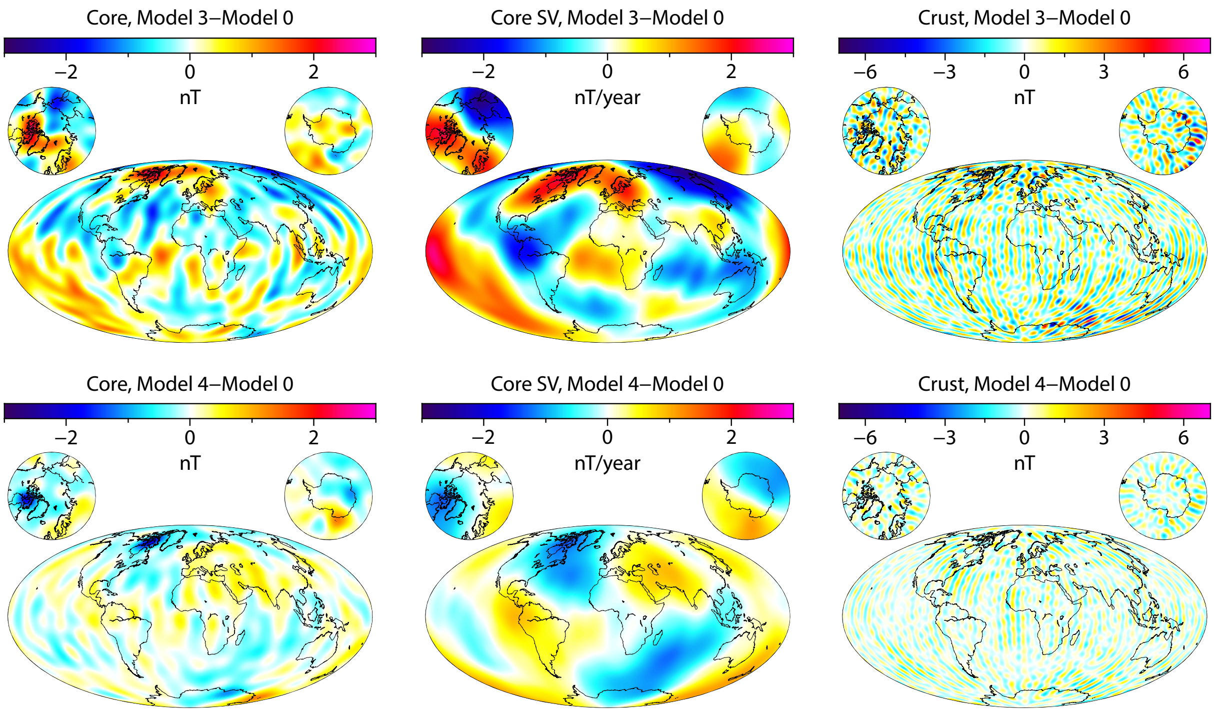

Figure 5. Similar to Figure 3, but for Models 3 and 4.

3.4 Influence of Data Selection According to *RC* Index

Next, we investigate the influence of data selection according to the time variations of the *RC* index, i.e. d*RC*/d*t*. Rapid changes in the *RC* index reflect rapid disturbances of the Earth's magnetosphere. This criterion excludes data during periods of enhanced ring current activity. We tested three data sets selected by $|dRC/dt| \le 2$ nT/h (Model 0), $|dRC/dt| \le 1$ nT/h (Model 5), $|dRC/dt| \le 3$ nT/h (Model 6). Results for these tests are presented in Table 4, Figures 6 and 7. These results are similar to those of the data selection according to the *Kp* index. A stricter data selection criterion leads to lower RMS misfits, while a looser data selection criterion leads to higher RMS misfits. However, as shown in Figures 6 and 7, the differences caused by changing the d*RC*/d*t* index in data selection are obviously larger, especially for the core SV field. When changing the d*RC*/d*t* index by 50% in data selection, the model uncertainties are in the ranges of ±3 nT, ±4 nT/year, and ±8 nT for the core, core SV, and crustal fields, respectively.

3.5 Influence of Data Selection According to E_m and IMF B_z

Finally, we investigate the influence of data selection according to merging electric field E_m and IMF B_z. In polar regions, there are complex ionospheric current systems such as the auroral electrojet and the field-aligned current that couples the ionosphere and magnetosphere. In our current field modeling framework, we don't co-estimate the ionospheric fields but try to minimize their contributions. First, we try to minimize the contribution of the low and mid-latitude EEJ and Sq currents by selecting dark-region data. Second, the polar current systems, particularly the field-aligned currents, primarily influence the direction of the magnetic field but have minimal impact on the scalar field intensity (Friis-Christensen et al., 2017). Therefore, we try to minimize the contribution of the polar current systems by using only scalar data. The merging electric field E_m (Newell et al., 2007), which is a function of the solar wind speed and the IMF, can efficiently monitor the strength of polar geomagnetic activity. Besides, it is suggested that the geomagnetic activity is much reduced during northward IMF ($B_z > 0$) (Ritter et al., 2004; Finlay et al., 2015). Therefore, applying data selection according to E_m and IMF B_z can further minimize the contribution of the polar current systems.

Here, we considered three data sets to investigate the effect of these data selection criteria. Compared to the reference Model 0, Models 7 and 8 were derived from data with and without data selection according to E_m and IMF B_z. Results are shown in Table 5, Figures 8 and 9. We have the following observations. First, without

Table 4. Similar to Table 2, but for magnetic field Models 0, 5 and 6.

Field	Model 0		Model 5		Model 6	
	Mean	RMS	Mean	RMS	Mean	RMS
F	−0.01	3.39	−0.00	3.33	−0.01	3.46
B_r	0.06	1.83	0.06	1.82	0.06	1.84
B_θ	0.01	2.62	0.01	2.57	0.01	2.66
B_ϕ	−0.04	2.26	−0.03	2.23	−0.05	2.28

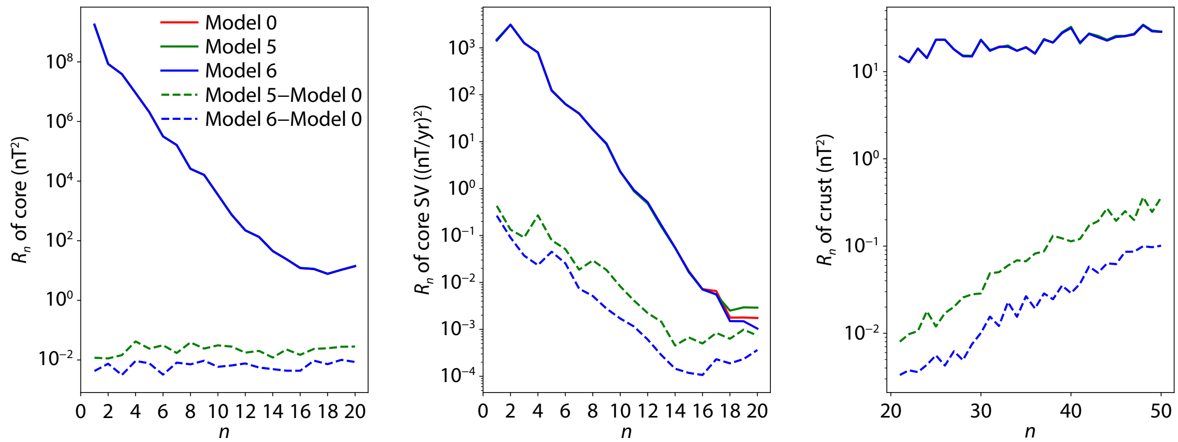

Figure 6. Similar to Figure 2, but for magnetic field Models 0, 5, and 6.

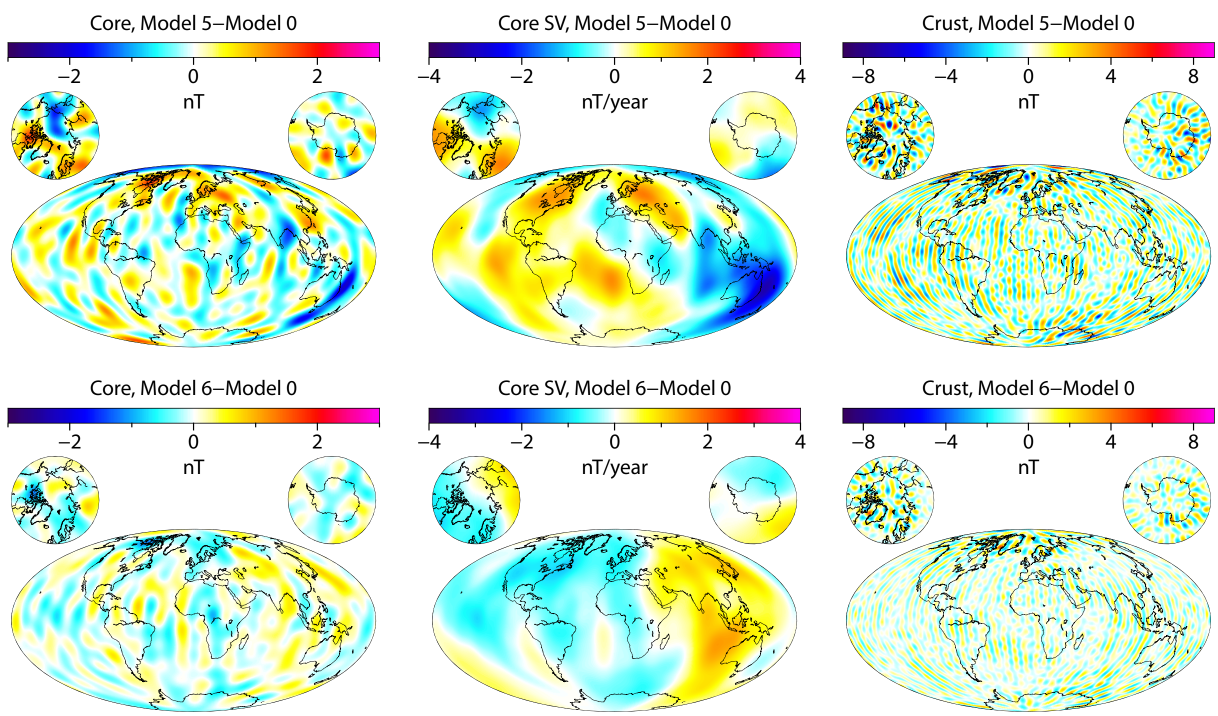

Figure 7. Similar to Figure 3, but for Models 5 and 6.

Table 5. Similar to Table 2, but for magnetic field Models 0, 7 and 8.

Field	Model 0		Model 7		Model 8	
	Mean	RMS	Mean	RMS	Mean	RMS
F	−0.01	3.39	−0.02	3.86	−0.01	3.57
B_r	0.06	1.83	0.06	1.89	0.06	1.81
B_θ	0.01	2.62	0.01	2.78	0.00	2.63
B_ϕ	−0.04	2.26	−0.05	2.39	−0.05	2.27

data selection according to E_m and IMF B_z, the RMS misfits of the vector field have only small changes, while those of the scalar field F increase more distinctly. Second, the largest field differences between models derived from data with and without data selection according to E_m and IMF B_z occurred at polar regions for the core and crustal fields. Since scalar data are used in polar regions while vector data are used in non-polar regions, these results indicate the sensitivity of E_m and IMF B_z indices on polar geomagnetic activity and current systems. These observations underscore the challenges in accurately modeling the internal magnetic field at high latitudes, emphasizing the necessity of co-estimating polar magnetic field models. When changing E_m and IMF B_z by 50% in

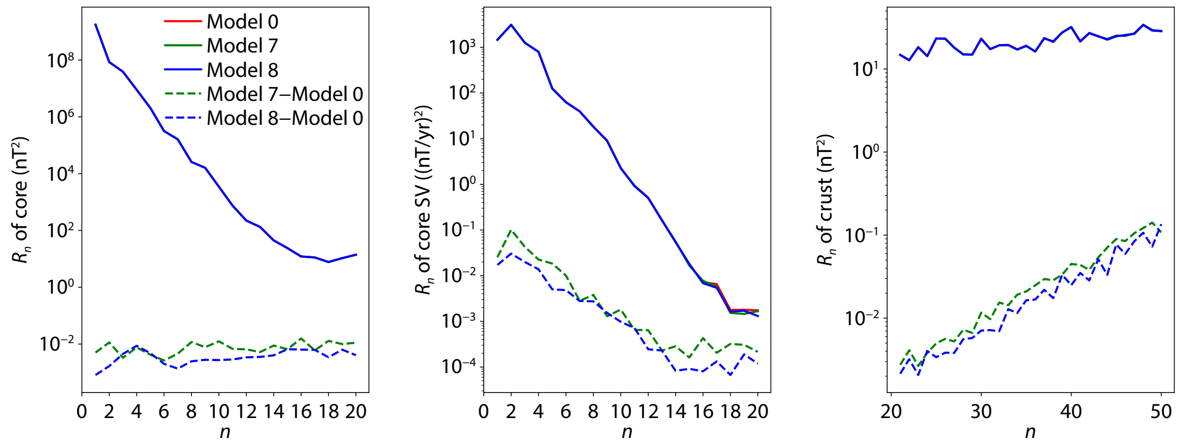

Figure 8. Similar to Figure 2, but for magnetic field Models 0, 7, and 8.

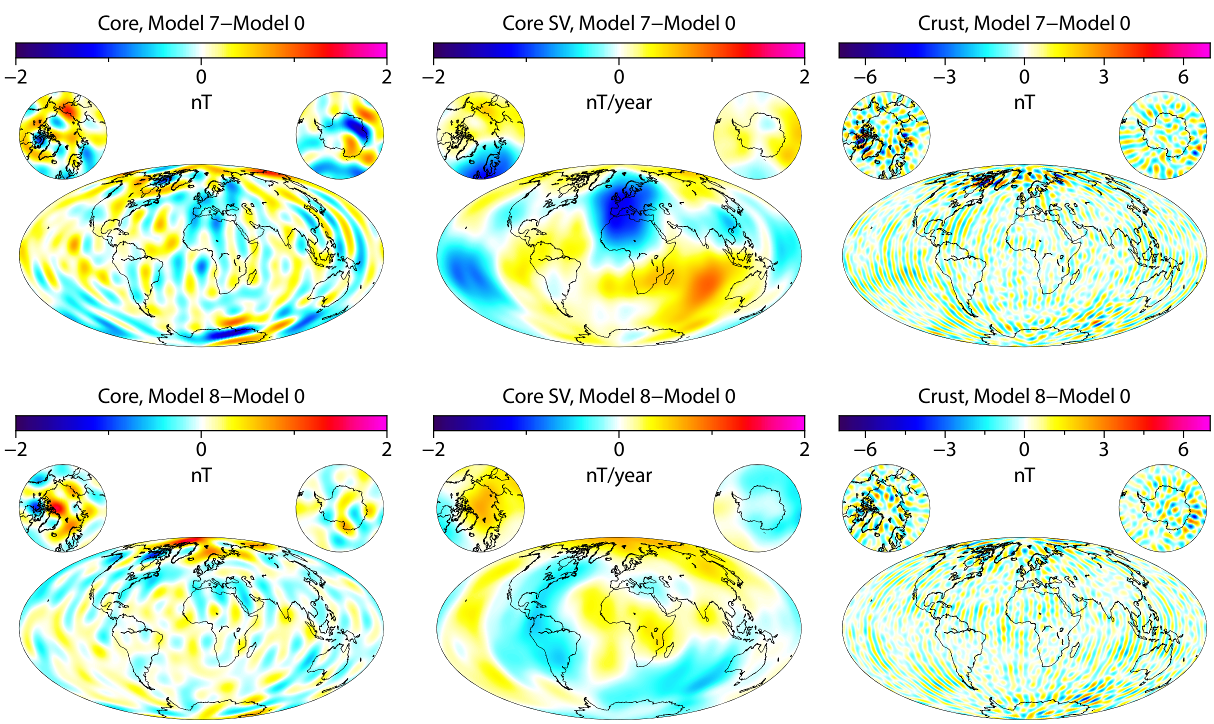

Figure 9. Similar to Figure 3, but for Models 7 and 8.

data selection, the model uncertainties are in the ranges of ±2 nT, ±2 nT/year, and ±6 nT for the core, core SV, and crustal fields, respectively. Therefore, uncertainties caused by data selection according to E_m and IMF B_z should also be considered when using magnetic field models at high latitudes.

4. Conclusions

Using the latest MSS-1 and Swarm satellite magnetic data, we conducted a series of field modeling experiments to examine the impact of different data selection criteria on internal geomagnetic field modeling. Our findings indicate that altering the threshold values of geomagnetic activity indices by 50% during data selection introduces uncertainties of approximately ±3 nT, ±4 nT/year, and ±8 nT for the core, SV, and crustal fields at Earth's surface, respectively. These uncertainties exceed the measurement accuracy of modern geomagnetic satellites, suggesting that they should be accounted for when utilizing the constructed magnetic field models.

To further mitigate the effects of current systems in the ionosphere and magnetosphere on internal field modeling, future work will focus on the following aspects. First, the gradient magnetic data from satellite measurements, which are less influenced by large-scale external field contributions, can be incorporated. The accurate East–West gradient of Earth's magnetic field, which can be derived from the low-inclination MSS-1 satellite magnetic data, will significantly improve internal geomagnetic field modeling. Additionally, extending our field modeling framework to co-estimate ionospheric fields will also benefit internal field modeling.

Acknowledgments

This work was supported by the National Natural Science Foundation of China (42250101) and the Macao Foundation. MSS-1 magnetic data are available at https://mss.must.edu.mo/data.html. Swarm magnetic data are available at http://swarm-diss.eo.esa.int or ftp://swarm-diss.eo.esa.int. We would like to thank Professor Keke Zhang for insightful discussions during the preparation of this manuscript.

References

Chulliat, A., Brown, W., Alken, P., Beggan, C., Nair, M., Cox, G., Woods, A., Macmillan, S., Meyer, B., and Paniccia, M. (2020). The US/UK World Magnetic Model for 2020–2025. UK: British Geological Survey.

Constable, C. G. (1988). Parameter estimation in non-Gaussian noise. *Geophys. J. Int.*, *94*(1), 131–142. https://doi.org/10.1111/j.1365-246x.1988.tb03433.x

De Boor, C. (1978). *A Practical Guide to Splines*. New York: Springer.

Farquharson, C. G., and Oldenburg, D. W. (1998). Non-linear inversion using general measures of data misfit and model structure. *Geophys. J. Int.*, *134*(1), 213–227. https://doi.org/10.1046/j.1365-246x.1998.00555.x

Finlay, C. C., Olsen, N., and Tøffner-Clausen, L. (2015). DTU candidate field models for IGRF-12 and the CHAOS-5 geomagnetic field model. *Earth Planets Space*, *67*(1), 114 https://doi.org/10.1186/s40623-015-0274-3

Finlay, C. C., Lesur, V., Thébault, E., Vervelidou, F., Morschhauser, A., and Shore, R. (2017). Challenges handling magnetospheric and ionospheric signals in internal geomagnetic field modelling. *Space Sci. Rev.*, *206*(1-4), 157–189. https://doi.org/10.1007/s11214-016-0285-9

Finlay, C. C., Kloss, C., Olsen, N., Hammer, M. D., Tøffner-Clausen, L., Grayver, A., and Kuvshinov, A. (2020). The CHAOS-7 geomagnetic field model and observed changes in the South Atlantic Anomaly. *Earth Planets Space*, *72*(1), 156 https://doi.org/10.1186/s40623-020-01252-9

Friis-Christensen, E., Finlay, C. C., Hesse, M., and Laundal, K. M. (2017). Magnetic field perturbations from currents in the dark polar regions during quiet geomagnetic conditions. *Space Sci. Rev.*, *206*(1-4), 281–297. https://doi.org/10.1007/s11214-017-0332-1

Lesur, V., Whaler, K., and Wardinski, I. (2015). Are geomagnetic data consistent with stably stratified flow at the core–mantle boundary?. *Geophys. J. Int.*, *201*(2), 929–946. https://doi.org/10.1093/gji/ggv031

Li, J. F., Lin, Y. F., and Zhang, K. (2024). Dynamic mode decomposition of the core surface flow inverted from geomagnetic field models. *Geophys. Res. Lett.*, *51*(1), e2023GL106362 https://doi.org/10.1029/2023gl106362

Matzka, J., Stolle, C., Yamazaki, Y., Bronkalla, O., and Morschhauser, A. (2021). The geomagnetic *Kp* index and derived indices of geomagnetic activity. *Space Wea.*, *19*(5), e2020SW002 https://doi.org/10.1029/2020sw002641

Maus, S., Manoj, C., Rauberg, J., Michaelis, I., and Lühr, H. (2010). NOAA/NGDC candidate models for the 11th generation International Geomagnetic Reference Field and the concurrent release of the 6th generation Pomme magnetic model. *Earth Planets Space*, *62*(10), 729–735. https://doi.org/10.5047/eps.2010.07.006

Maus, S., Nair, M. C., Poedjono, B., Okewunmi, S., Fairhead, D., Barckhausen, U., Milligan, P. R., and Matzka, J. (2012). High definition geomagnetic models: A new perspective for improved wellbore positioning. In *IADC/SPE Drilling Conference and Exhibition*. San Diego, California, USA: SPE. https://doi.org/10.2118/151436-ms

Newell, P. T., Sotirelis, T., Liou, K., Meng, C. I., and Rich, F. J. (2007). A nearly universal solar wind-magnetosphere coupling function inferred from 10 magnetospheric state variables. *J. Geophys. Res.: Space Phys.*, *112*(A1), A01206 https://doi.org/10.1029/2006ja012015

Olsen, N. (2002). A model of the geomagnetic field and its secular variation for epoch 2000 estimated from Ørsted data. *Geophys. J. Int.*, *149*(2), 454–462. https://doi.org/10.1046/j.1365-246x.2002.01657.x

Olsen, N., and Mandea, M. (2008). Rapidly changing flows in the Earth's core. *Nat. Geosci.*, *1*(6), 390–394. https://doi.org/10.1038/ngeo203

Olsen, N., Lühr, H., Sabaka, T. J., Mandea, M., Rother, M., Tøffner-Clausen, L., and Choi, S. (2006). CHAOS-a model of the Earth's magnetic field derived from CHAMP, Ørsted, and SAC-C magnetic satellite data. *Geophys. J. Int.*, *166*(1), 67–75. https://doi.org/10.1111/j.1365-246x.2006.02959.x

Olsen, N., Mandea, M., Sabaka, T. J., and Tøffner-Clausen, L. (2009). CHAOS-2-a geomagnetic field model derived from one decade of continuous satellite data. *Geophys. J. Int.*, *179*(3), 1477–1487. https://doi.org/10.1111/j.1365-246x.2009.04386.x

Olsen, N., Friis-Christensen, E., Floberghagen, R., Alken, P., Beggan, C. D., Chulliat, A., Doornbos, E., da Encarnaćão, J. T., Hamilton, B., … Visser, P. N. (2013). The Swarm satellite constellation application and research facility (SCARF) and Swarm data products. *Earth Planets Space*, *65*(11), 1189–1200. https://doi.org/10.5047/eps.2013.07.001

Olsen, N., Lü hr, H., Finlay, C. C., Sabaka, T. J., Michaelis, I., Rauberg, J., and Tøffner-Clausen, L. (2014). The CHAOS-4 geomagnetic field model. *Geophys. J. Int.*, *197*(2), 815–827. https://doi.org/10.1093/gji/ggu033

Purucker, M., Langlais, B., Olsen, N., Hulot, G., and Mandea, M. (2002). The southern edge of cratonic North America: Evidence from new satellite magnetometer observations. *Geophys. Res. Lett.*, *29*(15), 56-1–56-4. https://doi.org/10.1029/2001gl013645

Ritter, P., Lühr, H., Maus, S., and Viljanen, A. (2004). High-latitude ionospheric currents during very quiet times: Their characteristics and predictability. *Ann. Geophys.*, *22*(6), 2001–2014. https://doi.org/10.5194/angeo-22-2001-2004

Sabaka, T. J., Tøffner-Clausen, L., Olsen, N., and Finlay, C. C. (2020). CM6: A comprehensive geomagnetic field model derived from both CHAMP and Swarm satellite observations. *Earth Planets Space*, *72*(1), 80 https://doi.org/10.1186/s40623-020-01210-5

Wang, J., Yang, Y. Y., Zeren, Z., Wang, J., Wang, X., Luo, Y. X., and Shen, X. H. (2024). Preliminary geological interpretation of long-wavelength magnetic anomalies over China and surrounding regions. *Earth Planet. Phys.*, *8*(3), 445–458. https://doi.org/10.26464/epp2024025

Winch, D. E., Ivers, D. J., Turner, J. P. R., and Stening, R. J. (2005). Geomagnetism and Schmidt quasi-normalization. *Geophys. J. Int.*, *160*(2), 487–504. https://doi.org/10.1111/j.1365-246x.2004.02472.x

Xu, J. Y., Lin, Y. F., and Zhang, K. (2024). The influence of regularization on the geomagnetic core field modeling. *Rev. Geophys. Planet. Phys. (in Chinese)*, *55*(6), 719–732. https://doi.org/10.19975/j.dqyxx.2024-004

Yan, Q., and Yao, H. B. (2024). Recent geomagnetic storms observed by Macau Science Satellite-1. *Earth Planet. Phys.*, *8*(4), 565–569. https://doi.org/10.26464/epp2024047

Yang, Y. Y., Hulot, G., Vigneron, P., Shen, X. H., Zhima, Z., Zhou, B., Magnes, W., Olsen, N., Tøffner-Clausen, L., … Zhu, X. H. (2021). The CSES global geomagnetic field model (CGGM): An IGRF-type global geomagnetic field model based on data from the China Seismo-Electromagnetic Satellite. *Earth Planets Space*, *73*(1), 45 https://doi.org/10.1186/s40623-020-01316-w

Yao, H. B., Xu, J. Y., and Zhang, K. (2025). A method for simultaneously determining Earth's magnetic field and mantle conductivity models using MSS-1 and Swarm satellite magnetic data. *Phys. Earth Planet. Inter.*, *358*, 107296 https://doi.org/10.1016/j.pepi.2024.107296

Zhang, K. (2023). A novel geomagnetic satellite constellation: Science and applications. *Earth Planet. Phys.*, *7*(1), 4–21. https://doi.org/10.26464/epp2023019